UC Berkeley
UC Berkeley Previously Published Works

Title

Multifunctional Microelectro-Opto-mechanical Platform Based on Phase-Transition Materials

Permalink

https://escholarship.org/uc/item/9rc97006

Journal

Nano Letters, 18(3)

ISSN

1530-6984

Authors

Wang, Xi
Dong, Kaichen
Choe, Hwan Sung
et al.

Publication Date

2018-03-14

DOI

10.1021/acs.nanolett.7b04477

Peer reviewed

Multifunctional Microelectro-Opto-mechanical Platform Based on Phase-Transition Materials

Xi Wang,[†] Kaichen Dong,[†,‡,‖] Hwan Sung Choe,[†,‡] Huili Liu,[†,‡] Shuai Lou,[†] Kyle B. Tom,[†,‡] Hans A. Bechtel,[§] Zheng You,[‖] Junqiao Wu,[†,‡] and Jie Yao*[,†,‡]

[†]Department of Materials Science and Engineering, University of California, Berkeley, California 94720, United States

[‡]Materials Sciences Division and [§]Advanced Light Source Division, Lawrence Berkeley National Laboratory, Berkeley, California 94720, United States

[‖]State Key Laboratory of Precision Measurement Technology and Instruments, Department of Precision Instrument, Tsinghua University, Beijing 100084, People's Republic of China

S Supporting Information

ABSTRACT: Along with the rapid development of hybrid electronic−photonic systems, multifunctional devices with dynamic responses have been widely investigated for improving many optoelectronic applications. For years, microelectro-opto-mechanical systems (MEOMS), one of the major approaches to realizing multifunctionality, have demonstrated profound reconfigurability and great reliability. However, modern MEOMS still suffer from limitations in modulation depth, actuation voltage, or miniaturization. Here, we demonstrate a new MEOMS multifunctional platform with greater than 50% optical modulation depth over a broad wavelength range. This platform is realized by a specially designed cantilever array, with each cantilever consisting of vanadium dioxide, chromium, and gold nanolayers. The abrupt structural phase transition of the embedded vanadium dioxide enables the reconfigurability of the platform. Diverse stimuli, such as temperature variation or electric current, can be utilized to control the platform, promising CMOS-compatible operating voltage. Multiple functionalities, including an active enhanced absorber and a reprogrammable electro-optic logic gate, are experimentally demonstrated to address the versatile applications of the MEOMS platform in fields such as communication, energy harvesting, and optical computing.

KEYWORDS: *Microelectro-opto-mechanical systems, phase-transition materials, active enhanced absorber, reprogrammable electro-optic logic gate*
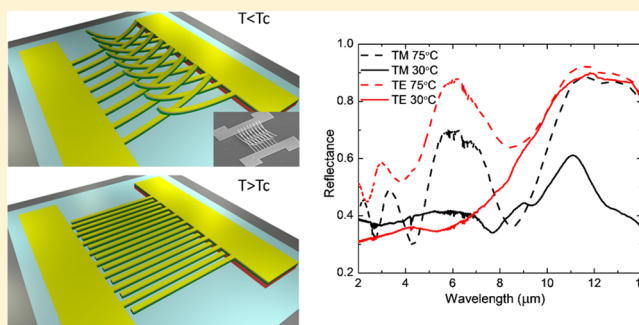
Dynamic functionalities in hybrid electronic−photonic systems are being widely pursued to further improve the system-level performance in optical communication and data processing.[1,2] While waveguide-based modulators are widely used in integrated silicon photonics,[3] optical modulators working in free space are also essential for practical optical applications, such as free-space optical communication,[4] beam diffraction,[5] interchip connection,[6] and light harvesting.[7] Free-space optical signal modulations have been realized by various mechanisms, including acousto-optic,[5] thermo-optic,[8] magneto-optic,[9] liquid-crystal, electro-optic, and micromechanical methods.[10−12] Among them, micro- and nanoelectro-opto-mechanical systems (MEOMS and NEOMS) have drawn tremendous attraction in recent years due to their reconfigurability, potential for further miniaturization, and great reliability[12,13] and thus endow novel and conventional materials with tunable or switchable functionalities. Currently, most MEOMS and NEOMS rely on electromagnetic forces (Coulomb, Ampere, Lorentz, and optical force) to reconfigure

the shape of optical-units and utilize elastic forces for restoration.[14−16] Conventional MEOMS are mostly micro-mirrors and -lenses with feature sizes much larger than their working wavelengths, which limit subwavelength miniaturization, thus making them not suitable for high-integration applications.[17] Additionally, the complex designs of such structures limit their functionality. The creation of MEOMS devices with subwavelength feature sizes, large modulation depths, simple on-chip electrical actuation, and design flexibility is in great demand.

To achieve that goal, modern MEOMS and NEOMS are integrated with subwavelength optics, such as nanobeams and meta-atoms.[1] To work at high operation frequencies (up to megahertz), some devices utilized electrostatic force for actuation. However, those devices are intrinsically limited by

either a low-transmission and -reflection modulation depth (<~10%)[14] or a large actuation voltage (>10 V).[18,19] These disadvantages make such devices unsuitable for applications such as wavelength demultiplexing[20] and dynamic filters.[21,22] Some other reconfigurable MEOMS and NEOMS are based on thermal expansion actuation,[23,24] in which a bimorph, a suspended structure (cantilever or double-clamped beam) consisting of two materials with different coefficients of thermal expansion (CTE), is typically used. Such structures achieve relatively better optical modulation depth (~50%) at the expense of large temperature variations (~200 K), implying high power consumption, restricted working environments, and low operation frequencies.[25,26] Therefore, both technologies fail to deliver satisfactory performance in all the aforementioned aspects.

Here, we demonstrate a new MEOMS design based on a phase-transition material, vanadium dioxide (VO_2), which has a reversible phase transition between an insulating (I) and a metallic (M) phase that is accompanied by an abrupt lattice expansion (M to I) or contraction (I to M) along the c_R axis of VO_2 crystals.[25] The I-to-M phase transition is triggered when the temperature increases beyond a critical temperature (T_c = 68 °C) slightly above room temperature.[27] The phase-transition-induced strains in single-crystal VO_2 samples and poly crystalline VO_2 films are 1% and 0.3%, respectively, much larger than the strains induced by thermal expansion (for ΔT = 10 K, the same temperature variation as the hysteresis width of VO_2) and typical piezoelectric actuations.[25] All of the above features indicate that VO_2 is an ideal actuation material for MEOMS/NEOMS. However, the mismatched built-in stresses in conventional VO_2 actuators (mostly bilayer) resulted in undesirable large curvatures ubiquitously observed in previously reported works.[25,28] This prevents VO_2 from being further utilized in practical MEOMS and NEOMS devices. Recently, we have demonstrated a design procedure based on multilayer structures that can arbitrarily manipulate the curvatures of VO_2 cantilever actuators at both M and I phases.[29] This circumvents the above hindrance and thus enables a new platform for MEOMS and NEOMS devices—multifunctional VO_2 cantilever actuator arrays. We designed and characterized MEOMS devices based on this new platform, which fits the requirements of good MEOMS devices summarized above.

Our MEOMS devices can be operated by various stimuli, such as global temperature, Joule heating, or potentially by a photothermal method.[30] Unlike conventional VO_2-based optical devices whose tunable properties are largely dependent on and limited by the optical properties of the VO_2 itself,[31,32] the performance of our new MEOMS devices mainly relies on the reconfiguration of metallic structures, while VO_2 is integrated as the mechanical actuation material. As such, large flexibility in materials selection and working wavelengths, as well as versatile functionality, can be achieved.

The schematics of the first MEOMS device are illustrated in Figure 1a. All geometric parameters are readily tunable. The structure was fabricated on a Si substrate covered by a 200 nm thick platinum (Pt) layer. The cantilevers are designed to be curved upward at room temperature (I phase) and flat at temperatures above T_c (M phase). To achieve that design, we constructed a trilayer structure containing VO_2, chromium (Cr), and gold (Au) layers. By calculating the curvatures of the trilayer cantilever with different thickness ratios, the thicknesses of VO_2, Cr, and Au layers were determined to be 200, 41, and 65 nm, respectively.[29] The lengths of fabricated cantilevers are
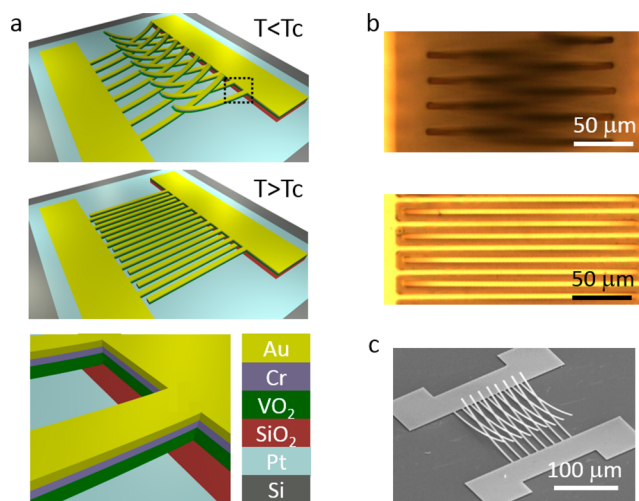

Figure 1. (a) Schematics of the MEOMS device showing curved cantilevers at room temperature (top) and flat cantilevers at temperature above T_c (mid). The bottom panel shows the layered structure in the dotted rectangle in the top panel; (b) top view of a MEOMS device at room temperature (top) and 75 °C (bottom) under an optical microscope; (c) a SEM image of an as-fabricated MEOMS device.

chosen to be 200 μm. The period of the cantilever array is fixed to 8 μm. The cantilevers are supported by two rectangular anchors facing each other, which are also large enough to prevent peel-off during the removal of the sacrificial material (SiO_2) by wet etching. Detailed fabrication procedures are summarized in the Methods section.

The reconfigurable behavior of the MEOMS device before and after the phase transition of VO_2 can be examined conveniently under an optical microscope. At room temperature, all cantilevers bend up uniformly (top panel of Figure 1b). The array appears dark due to the deflection of light by the bent cantilevers. When the temperature is increased above T_c, the VO_2 layer in the cantilevers transforms from the I phase into the M phase with an in-plane shrinkage, driving the cantilevers to bend downward, eventually attaining a flat state (bottom panel of Figure 1b), which is verified by the strong reflection from the device. Figure 1c shows the SEM image of an as-fabricated MEOMS device at room temperature, further confirming the uniform curvature of the fabricated cantilevers, which is suitable for optical applications.

The reflection spectra of fabricated MEOMS devices were characterized by an FTIR system with details summarized in the Methods section. The normalized reflectance of one sample with a 3 μm cantilever width is shown in Figure 2a. The MEOMS device shows dramatic modulation over a wide wavelength range before and after the phase transition of VO_2 for both TM (electric field perpendicular to the direction of the cantilevers) and TE (electric field parallel to the direction of the cantilevers) polarized incident light.

When the cantilevers are in the flat state ($T > T_c$), the MEOMS device serves as a diffraction grating with a back mirror, contributing to the spectra oscillation over the entire spectrum range. At longer wavelengths (>10 μm), there is no high-order diffracted beam. The zeroth order beam contains the majority of the energy and is collected by the objective lens; hence, the reflectance is relatively high. The spectra oscillations exhibit shorter periods at shorter wavelengths, which is similar
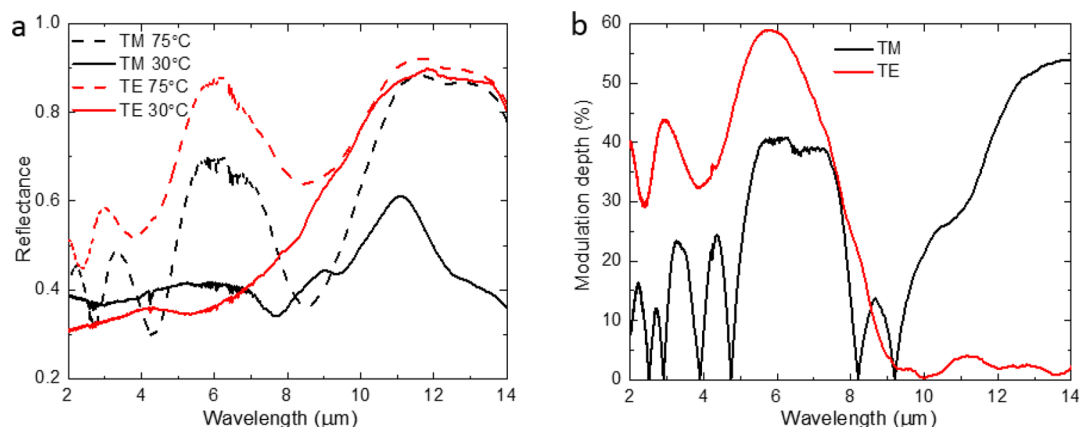
Figure 2. (a) Reflection spectra and (b) corresponding modulation depths of a MEOMS device.
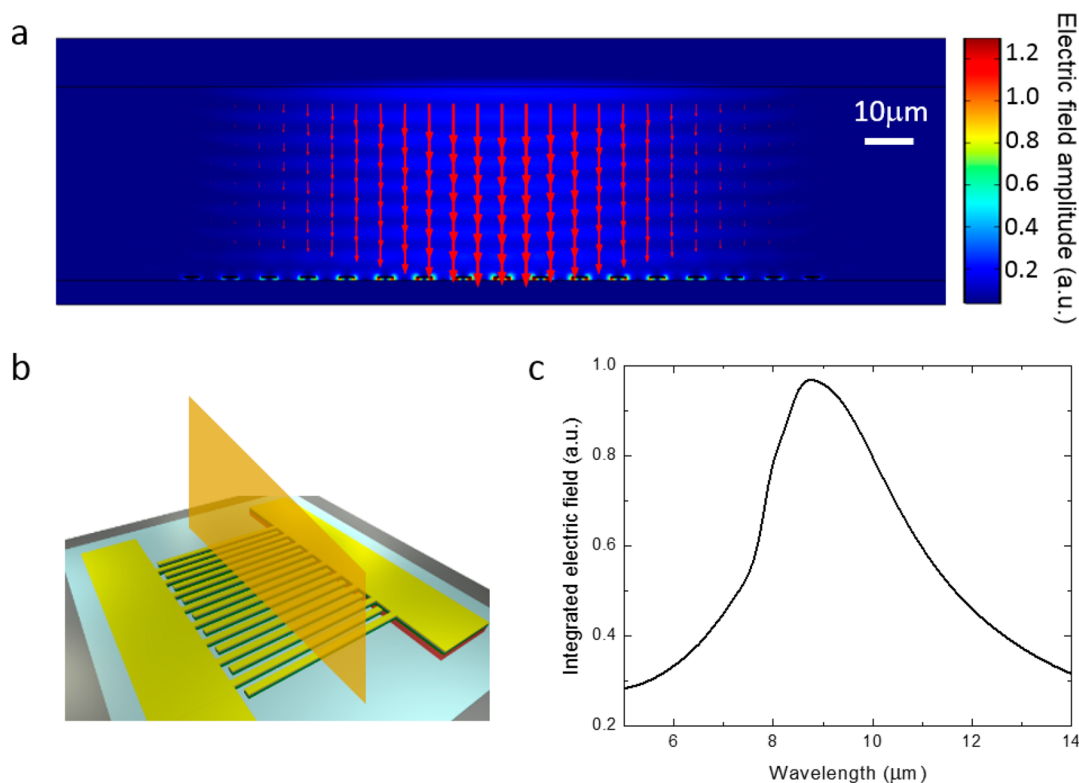

Figure 3. (a) Simulation results of electric field amplitude and Poynting vectors (red arrows) near a MEOMS device under 8.8 μm illumination showing the enhanced absorption behavior; (b) the relation between the simulated 2D plane and a MEOMS device; (c) wavelength-dependent integrated electric field at the center region between the cantilevers and the Pt surface.

to the oscillation trend of the diffraction efficiency of the zeroth order, as seen in previously reported results.[33]

When the cantilevers are curved ($T < T_c$), the MEOMS device splits into two tilted and curved gratings with a doubled period and a halved filling ratio compared with those in the flat state. For TE-polarized incident light at longer wavelengths, the curvature of the cantilevers is not significant compared to the incident wavelength, so most of the light is still reflected by the cantilevers. At shorter wavelengths, more light is reflected by the curved cantilevers, showing a reduced zeroth-order reflectance. For TM-polarized incident light, surface plasmon polaritons and localized surface plasmons are excited around the cantilevers. As a result, relatively low reflectance is observed.

The modulation capability of our MEOMS device is quantified by its modulation depth, which is defined by

$\frac{|R_{flat} - R_{curved}|}{R_{max}}$ and plotted in Figure 2b. The modulation depths are greater than 50% at multiple wavelength ranges (between 5 and 7 μm for TE polarized light and 12 to 14 μm for TM-polarized light). This is comparable with the state-of-the-art MEOMS and NEOMS devices in the same wavelength range.[18,19] Such a large optical modulation depth of our MEOMS devices already promise various applications, including selective wavelength reflection spectrum filters and diffraction gratings. Other applications and diversity in responsive stimuli are demonstrated below.

Active Enhanced Absorber. Besides having advantages as an active diffraction grating and a high-modulation-depth spectral filter, the above MEOMS device provides us a platform on which active optical devices with multiple functions can be
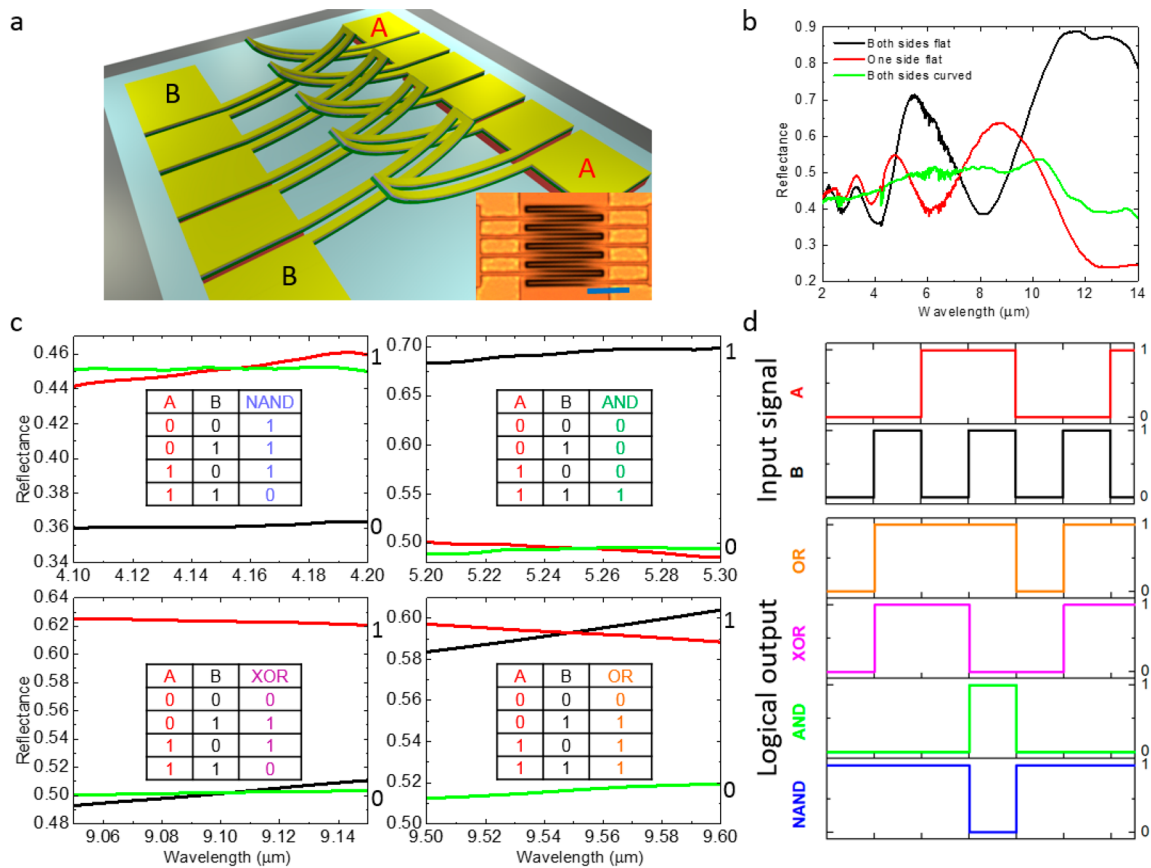
Figure 4. (a) Schematic and top-view optical image (inset) of a U-shape MEOMS device (scale bar: 100 μm); (b) reflection spectra of a U-shape MEOMS device at different states; (c) enlarged reflection spectra at wavelengths corresponding to certain logic gates; (d) demonstration of logic operation for four logic gates shown in panel c. A pair of input signals show 0/1 logic input conditions, corresponding to 0/3.6 mA current flows on A and B side, respectively.

realized. Here, we conduct experiments and numerical simulations to illustrate its application as an active enhanced absorber.

It is well-known that metal−semiconductor−metal grating structures can work as enhanced absorbers, which have been utilized to improve the efficiency of solar cells as well as the sensitivity of photodetectors.[34] With a homogeneous metal film blocking the transmission (i.e., Pt in our experiment), absorption information can be obtained from reflection measurements. For the MEOMS device characterized in Figure 2a, the enhanced absorption wavelength is 8.8 μm, seen as a reflection dip in the spectrum. Using simulations, we can easily identify the enhanced absorption behavior and understand the physics that leads to the enhanced absorption. As seen in Figure 3a, when the incident wavelength is 8.8 μm, there are no horizontal components for the Poynting vectors and the interference caused by reflectance is very weak. The relation between the simulated two-dimensional (2D) plane and the MEOMS device is shown in Figure 3b. We further calculated the wavelength-dependent plot (Figure 3c) by integrating the electric field inside the gap between the cantilevers and the Pt surface at the center of the illumination area (illuminated by a Gaussian beam with $\omega_0 = 50$ μm). The Figure 3c clearly shows the enhanced absorption at 8.8 μm. When a device is specifically designed for this individual functionality, the performance of the enhanced absorption can be further optimized by tuning the parameters of the structure. By actively controlling the curved and flat states of the MEOMS

device, the enhanced absorption behavior can be tuned, which will greatly boost the device performance in fields such as microfluidics[35] or biomolecule detection.[36]

Electrical Control. MEOMS devices controlled by electrical signals are in great demand in electro-photonic systems for programmable control and integrability with electrical circuits.[2] To minimize heat dissipation and reduce power consumption, the cantilevers are optimized into a U-shape structure, which allows electrical current to flow through the cantilevers directly, as shown in Figure 4a. Either side of the MEOMS device can be separately Joule-heated using the corresponding electrodes (A or B). The ON threshold for the phase transition of VO_2 to drive all cantilevers on either side to be completely flat is experimentally determined to be ∼3.6 mA, while the substrate was kept at room temperature. The minimum voltage to operate the MEOMS devices is ∼0.5 V, compatible with the state-of-art voltage level (∼1 V) of CMOS circuits,[37] facilitating the integration of our MEOMS devices into CMOS systems for further applications of "photonics on a chip".[2,38,39]

Reprogrammable Electro-optic Logic Gate. Electric logic devices have played a critical role in the rapid development of the semiconductor industry. In recent years, with the rise of optical communication and sensing, electro-optic logic gates have been widely investigated for direct optical signal processing.[40] Currently, there are two main types of electro-optic logic gates: Mach−Zehnder interferometers[41] and microring resonators.[42] As a result of constrained flexibility in the design process, both of the above-mentioned types are

limited by fixed logical operation after fabrication. In contrast, our MEOMS devices serve as reprogrammable electro-optic logic gates with flexibility in design. After fabrication, the logical operation of one MEOMS device is reprogrammable by simply adjusting its working wavelengths. Here, we use a MEOMS device with its reflection spectra shown in Figure 4b as a demonstration.

To convert both electrical and optical signals to logic inputs and outputs, we define that (1) when the electric current flowing through one side is larger than 3.6 mA, which is the threshold current for the flat state of the MEOMS device, the input is logic 1; (2) when the electric current flowing through one side is smaller than 1.5 mA (the minimum current necessary to start driving the cantilevers down), the input is logic 0. Similarly, logic 1 and 0 of the reflected optical signal (output) is defined by its reflectance and summarized in Figure 4c for different operation wavelengths. It is obvious that the logic operation at these wavelengths is completely controlled by the curved/flat states of the MEOMS device, which is fundamentally manipulated by the input electrical signals (heating currents). In this way, the MEOMS device serves as a reprogrammable electro-optic logic gate. The relationship between the input electrical signals and the output optical signals is summarized in Figure 4d. NAND, AND, XOR, and OR gates are successfully demonstrated at wavelengths of 4.15, 5.25, 9.1, and 9.55 μm, respectively. Their logic operations are summarized in the tables in Figure 4c. The working wavelengths and logic gate performance are completely designable during the fabrication process by varying the parameters of the MEOMS device.

Discussion. It is worth mentioning that, though our MEOMS devices were demonstrated in the mid-infrared wavelength region, there is no fundamental limit for those devices to be scaled down. Optical properties of materials such as VO_2, Au, Cr, and Pt do not change with size or geometric changes of the devices before they reach quantum regime. In contrast, the optical performance of our MEOMS devices can be adjusted through scaling or altering the geometry of the cantilevers, which is similar to other metamaterials and gratings that have been discussed in previous works.[43,44] For example, when the width of the cantilevers decreases, the enhanced absorption wavelength becomes shorter. As for the mechanical properties, even if the VO_2-based actuator is scaled-down to subμm, the physics of the VO_2 phase transition will remain the same, and the VO_2 will retain its mechanical actuation capability. Our current devices have demonstrated ~50% modulation depths above the wavelength of 1.43 μm (Figure S1), covering important wavelengths for optical communications. With further miniaturization, our MEOMS platform can be potentially utilized for applications in the visible wavelength region. In fact, VO_2 nanoactuators with scales down to 120 nm have been reported.[45]

In conclusion, we demonstrated a multifunctional MEOMS platform with greater than 50% light modulating capabilities and multiple control methods, including global heating, Joule heating, and, potentially, photothermal excitation. This platform is based on a specially designed cantilever array, with each cantilever consisting of VO_2, Cr, and Au nanolayers and actuated by the phase-transition-induced strain of the embedded VO_2. Based on this platform, versatile MEOMS devices were fabricated and demonstrated with multiple functionalities, which include selective wavelength reflection spectrum filters, diffraction gratings, enhanced absorbers,

reprogrammable electro-optic logic gates, and, potentially, active surface wave couplers (see the Supporting Information) near room temperature. The performance of the MEOMS devices can be further optimized for individual functionalities by refining the design, optimizing the VO_2 quality, and doping.[46] This MEOMS platform paves the way for a wide variety of practical MEOMS devices with versatile dynamic functionalities and high performance for future electronic–photonic systems.

Methods. *Fabrication.* 10 nm Cr and 200 nm Pt were deposited on a Si substrate by E-beam evaporation. Then, they were covered by plasma enhanced chemical vapor deposited (PECVD) SiO_2 as the sacrificial layer. Subsequently, pulsed laser deposition (PLD) was used to deposit 200 nm VO_2 onto the PECVD SiO_2. A krypton fluoride excimer laser (λ = 248 nm) and a VO_2 target (99%) were used for the PLD. The fluence and the repetition rate of the pulsed laser were 320 mJ and 5 Hz, respectively. The oxygen pressure was 5 mTorr, and the substrate temperature was kept at 575 °C during the VO_2 deposition. After the patterning of S1818 photoresist by photolithography, 41 nm Cr and 65 nm Au were deposited by E-beam evaporation and patterned by lift-off. Reactive ion etching (RIE) was utilized to remove the uncovered VO_2 layer, where patterned Au/Cr served as masks. Finally, Au/Cr/VO_2 cantilevers were released by buffered oxide etchant (BOE, 5:1) wet etching and critical point drying.

Characterization. The reflection spectra of fabricated MEOMS devices were characterized by an Agilent Cary 670 FTIR spectrometer and Agilent Cary 620 microscope system with a 15× objective lens (numerical aperture of 0.62) and a blade aperture (70 μm × 140 μm) selecting the center part of each MEOMS device. The aperture width along the direction of the cantilevers is chosen to be 70 μm to prevent the tips of the cantilevers from entering the characterization region at the I phase. The MEOMS devices were placed on a customized closed-loop thermal stage to accurately control the substrate temperature by a global heating method. The thermal stage, consisting of two Kapton insulated flexible heaters, one Pt temperature sensor, and a copper heat sink, is controlled by a Lakeshore 321 temperature controller. Reflection spectra at 30 °C (I phase, curved) and 75 °C (M phase, flat) were measured and normalized to the reflection spectrum of a 300 nm thick gold film. Joule heating experiments were carried out by connecting the electrodes of MEOMS devices to a DC power supply (BK Precision 1739, 30 V/1 A) using tungsten probes manipulated by Quarter Research and Development Model XYZ 300T micro-positioners.

Simulation. 2D simulations were performed using COMSOL Multiphysics. A total of 17 trilayer rectangles (width of 3 μm and heights of 200, 41, and 65 nm, respectively) imitating the 17 cantilevers in one MEOMS device were placed 500 nm above a Pt substrate with a period of 8 μm. A Gaussian beam (ω_0 = 50 μm) illuminated normally toward the center of the cantilevers. The optical properties of Au, Cr, and Pt were taken from previous reports.[47,48] The optical properties of VO_2 are extrapolated from ref 49. Perfect matched layers were used to surround the simulation space.

■ ASSOCIATED CONTENT

Ⓢ Supporting Information

The Supporting Information is available free of charge on the ACS Publications website at DOI: 10.1021/acs.nanolett.7b04477.

Figures showing FTIR measurement of a MEOMS device, simulation results, and power flow and experimental details. (PDF)

■ AUTHOR INFORMATION

Corresponding Author

*E-mail: yaojie@berkeley.edu.

ORCID

Xi Wang: 0000-0002-5066-0088

Kaichen Dong: 0000-0001-5334-4243

Junqiao Wu: 0000-0002-1498-0148

Author Contributions

X.W. and K.D. contributed equally to this work. X.W., K.D., J.W. and J.Y. conceived the idea and designed the experiments. K.D., H.S.C., X.W., H.L., and S.L. fabricated the MEOMS devices. X.W. and H.A.B. conducted the characterization experiments. X.W. performed simulations. All authors contributed to data analysis and interpretation. X.W., K.D., and J.Y. wrote the paper, and all authors provided feedback.

Notes

The authors declare no competing financial interest.

■ REFERENCES

(1) Zheludev, N. I.; Kivshar, Y. S. *Nat. Mater.* **2012**, *11*, 917−924.

(2) Sun, C.; Wade, M. T.; Lee, Y.; Orcutt, J. S.; Alloatti, L.; Georgas, M. S.; Waterman, A. S.; Shainline, J. M.; Avizienis, R. R.; Lin, S.; et al. *Nature* **2015**, *528*, 534−538.

(3) Jalali, B.; Fathpour, S. *J. Lightwave Technol.* **2006**, *24*, 4600−4615.

(4) LURYI, S.; GOUZMAN, M. *Int. J. High Speed Electron. Syst.* **2006**, *16*, 559−566.

(5) Donley, E. A.; Heavner, T. P.; Levi, F.; Tataw, M. O.; Jefferts, S. R. *Rev. Sci. Instrum.* **2005**, *76*, 063112.

(6) Goodman, J. W.; Leonberger, F. J.; Kung, S.-Y.; Athale, R. A. *Proc. IEEE* **1984**, *72*, 850−866.

(7) Herek, J. L.; Wohlleben, W.; Cogdell, R. J.; Zeidler, D.; Motzkus, M. *Nature* **2002**, *417*, 533.

(8) Haché, A.; Allogho, G.-G. *Opt. Commun.* **2011**, *284*, 1656−1660.

(9) Williamson, L. A.; Chen, Y.-H.; Longdell, J. J. *Phys. Rev. Lett.* **2014**, *113*, 203601.

(10) Steinmeyer, G. *Journal of Optics A: Pure and Applied Optics* **2003**, *5*, R1.

(11) Wu, M. C.; Lin, L. Y.; Lee, S. S.; Pister, K. S. J. *Sens. Actuators, A* **1995**, *50*, 127−134.

(12) Fan, K.; Padilla, W. J. *Materials Today* **2015**, *18* (1), 39.

(13) Zheludev, N. I.; Plum, E. *Nat. Nanotechnol.* **2016**, *11*, 16−22.

(14) Ou, J.-Y.; Plum, E.; Zhang, J.; Zheludev, N. I. *Nat. Nanotechnol.* **2013**, *8*, 252−255.

(15) Padilla, W. J.; Taylor, A. J.; Highstrete, C.; Lee, M.; Averitt, R. D. *Phys. Rev. Lett.* **2006**, *96*, 107401.

(16) Neilson, D. T.; Aksyuk, V. A.; Arney, S.; Basavanhally, N. R.; Bhalla, K. S.; Bishop, D. J.; Boie, B. A.; Bolle, C. A.; Gates, J. V.; Gottlieb, A. M., et al. In *Fully Provisioned 112 × 112 Micro-Mechanical Optical CrossConnect With 35.8Tb/s Demonstrated Capacity*; Optical Fiber Communication Conference, Baltimore, Maryland, 2000/03/07, 2000; Optical Society of America: Baltimore, MD, p PD12.

(17) Washburn, A. L.; Bailey, R. C. *Analyst* **2011**, *136*, 227−236.

(18) Liu, X.; Padilla, W. J. *Adv. Opt. Mater.* **2013**, *1*, 559−562.

(19) Zhao, X. G.; Fan, K. B.; Zhang, J. D.; Keiser, G. R.; Duan, G. W.; Averitt, R. D.; Zhang, X. *Microsystems & Nanoengineering* **2016**, *2*, 16025.

(20) Agrawal, G. P.; Radic, S. *IEEE Photonics Technol. Lett.* **1994**, *6*, 995−997.

(21) d'Alessandro, A.; Donisi, D.; De Sio, L.; Beccherelli, R.; Asquini, R.; Caputo, R.; Umeton, C. *Opt. Express* **2008**, *16*, 9254−9260.

(22) Wang, X.; Gong, Z.; Dong, K.; Lou, S.; Slack, J.; Anders, A.; Yao, J. *Opt. Express* **2016**, *24*, 20365−20372.

(23) Tao, H.; Strikwerda, A. C.; Fan, K.; Padilla, W. J.; Zhang, X.; Averitt, R. D. *Phys. Rev. Lett.* **2009**, *103*, 147401.

(24) Ou, J. Y.; Plum, E.; Jiang, L.; Zheludev, N. I. *Nano Lett.* **2011**, *11*, 2142−2144.

(25) Liu, K.; Cheng, C.; Cheng, Z.; Wang, K.; Ramesh, R.; Wu, J. *Nano Lett.* **2012**, *12*, 6302−6308.

(26) Liu, K.; Cheng, C.; Suh, J.; Tang-Kong, R.; Fu, D.; Lee, S.; Zhou, J.; Chua, L. O.; Wu, J. *Adv. Mater.* **2014**, *26*, 1746−1750.

(27) Barker, A. S.; Verleur, H. W.; Guggenheim, H. J. *Phys. Rev. Lett.* **1966**, *17*, 1286.

(28) Merced, E.; Tan, X.; Sepulveda, N. *J. Microelectromech. Syst.* **2014**, *23*, 1073−1083.

(29) Dong, K.; Lou, S.; Choe, H. S.; Liu, K.; You, Z.; Yao, J.; Wu, J. *Appl. Phys. Lett.* **2016**, *109*, 023504.

(30) Lysenko, S.; Rúa, A.; Vikhnin, V.; Fernández, F.; Liu, H. *Phys. Rev. B: Condens. Matter Mater. Phys.* **2007**, *76*, 035104.

(31) Driscoll, T.; Palit, S.; Qazilbash, M. M.; Brehm, M.; Keilmann, F.; Chae, B.-G.; Yun, S.-J.; Kim, H.-T.; Cho, S. Y.; Jokerst, N. M. *Appl. Phys. Lett.* **2008**, *93*, 024101.

(32) Goldflam, M. D.; Driscoll, T.; Chapler, B.; Khatib, O.; Jokerst, N. M.; Palit, S.; Smith, D. R.; Kim, B.-J.; Seo, G.; Kim, H.-T. *Appl. Phys. Lett.* **2011**, *99*, 044103.

(33) Golub, M. A.; Hutter, T.; Ruschin, S. *Appl. Opt.* **2010**, *49*, 1341−1349.

(34) Liu, K.; Zeng, B.; Song, H.; Gan, Q.; Bartoli, F. J.; Kafafi, Z. H. *Opt. Commun.* **2014**, *314*, 48−56.

(35) Kasirga, T. S.; Ertas, Y. N.; Bayindir, M. *Appl. Phys. Lett.* **2009**, *95*, 214102.

(36) Youn, S.-W.; Okuyama, C.; Takahashi, M.; Maeda, R. *J. Mater. Process. Technol.* **2008**, *201*, 548−553.

(37) Lee, J. O.; Song, Y.-H.; Kim, M.-W.; Kang, M.-H.; Oh, J.-S.; Yang, H.-H.; Yoon, J.-B. *Nat. Nanotechnol.* **2013**, *8*, 36−40.

(38) Barwicz, T.; Byun, H.; Gan, F.; Holzwarth, C. W.; Popovic, M. A.; Rakich, P. T.; Watts, M. R.; Ippen, E. P.; Kaertner, F. X.; Smith, H. I.; et al. *Journal of Optical Networking* **2007**, *6*, 63−73.

(39) Fischer, A. C.; Forsberg, F.; Lapisa, M.; Bleiker, S. J.; Stemme, G.; Roxhed, N.; Niklaus, F. *Microsystems & Nanoengineering* **2015**, *1*, 15005.

(40) Hardy, J.; Shamir, J. *Opt. Express* **2007**, *15*, 150−165.

(41) Reis, C.; Chattopadhyay, T.; Andre, P.; Teixeira, A. *Appl. Opt.* **2012**, *51*, 8693−8701.

(42) Zhang, L.; Ji, R.; Jia, L.; Yang, L.; Zhou, P.; Tian, Y.; Chen, P.; Lu, Y.; Jiang, Z.; Liu, Y.; et al. *Opt. Lett.* **2010**, *35*, 1620−1622.

(43) Palmer, C.; Loewen, E. G. *Diffraction grating handbook*; Newport Corporation: Irvine, CA, 2005.

(44) Cai, W.; Shalaev, V. *Optical metamaterials: fundamentals and applications*; Springer Science & Business Media: New York, 2009.

(45) Karl, H.; Peyinghaus, S. C. *Nucl. Instrum. Methods Phys. Res., Sect. B* **2015**, *365*, 75−78.

(46) Ma, H.; Hou, J.; Wang, X.; Zhang, J.; Yuan, Z.; Xiao, L.; Wei, Y.; Fan, S.; Jiang, K.; Liu, K. *Nano Lett.* **2017**, *17*, 421−428.

(47) Olmon, R. L.; Slovick, B.; Johnson, T. W.; Shelton, D.; Oh, S.-H.; Boreman, G. D.; Raschke, M. B. *Phys. Rev. B: Condens. Matter Mater. Phys.* **2012**, *86*, 235147.

(48) Rakić, A. D.; Djurišić, A. B.; Elazar, J. M.; Majewski, M. L. *Appl. Opt.* **1998**, *37*, 5271−5283.

(49) Chen, Z.; Wang, X.; Qi, Y.; Yang, S.; Soares, J. A. N. T.; Apgar, B. A.; Gao, R.; Xu, R.; Lee, Y.; Zhang, X.; et al. *ACS Nano* **2016**, *10*, 10237−10244.